

Associations between angiogenic factors and intravoxel incoherent motion-derived parameters in diffusion-weighted magnetic resonance imaging of breast cancer

Youn Joo Lee, MD^a, Sung Hun Kim, MD^{b,*} , Bong Joo Kang, MD^b, Yo Han Son, PhD^c, Robert Grimm, PhD^d

Abstract

Intravoxel incoherent motion (IVIM) diffusion-weighted magnetic resonance imaging (MRI) can be used to estimate perfusion-related parameters, but these parameters may differ, based on the curve-fitting algorithm used for IVIM. Microvessel density (MVD) and vascular endothelial growth factor (VEGF) status are used as angiogenic factors in breast cancer. We aimed to investigate the relationship between MVD, VEGF, and intravoxel incoherent motion (IVIM)-derived parameters, obtained by 4 curve-fitting algorithms, in patients with invasive breast cancers.

This retrospective study investigated IVIM-derived parameters, D (ie, tissue diffusivity), D^* (ie, pseudodiffusivity), and f (ie, perfusion fraction), of 55 breast cancers, using 10 b values (range, 0–800 s/mm²) and 4 curve-fitting algorithms: algorithm 1, linear fitting of D and f first, followed by D^* ; algorithm 2, linear fitting of D and f and nonlinear fitting of D^* ; algorithm 3, linear fitting of D and f , linear fitting of D^* , and ignoring D contribution for low b values; and algorithm 4, full nonlinear fitting of D , f , and D^* . We evaluated whole-tumor histograms of D , f , and D^* for their association with MVD and VEGF.

D^*_{10} , D^*_{25} , D^*_{50} , D^*_{mean} , D^*_{75} , D^*_{90} , f_{10} , and f_{25} , derived using algorithm 3, were associated with VEGF expression ($P = .043$, $P = 0.012$, $P = .019$, $P = .024$, $P = .044$, $P = .041$, $P = .010$, and $P = .005$, respectively). However, no correlation existed between MVD and IVIM-derived parameters.

Perfusion-related IVIM parameters obtained by curve-fitting algorithm 3 may reflect VEGF expression.

Abbreviations: ADC = apparent diffusion coefficient, DWI = diffusion-weighted imaging, IVIM = intravoxel incoherent motion, MVD = microvascular density, VEGF = vascular endothelial growth factor.

Keywords: breast neoplasm, diffusion-weighted imaging, intravoxel incoherent motion, magnetic resonance imaging

Editor: Neeraj Lalwani.

The statistical consultation was supported by Department of Biostatistics of the Catholic Research Coordinating Center, Catholic Medical Center, South Korea. This work was supported by grants from the National Research Foundation of Korea (NRF-2019R1A2C1085809).

The authors report no conflicts of interest.

The datasets generated during and/or analyzed during the current study are available from the corresponding author on reasonable request.

^aDepartment of Radiology, Daejeon St. Mary's Hospital, Daejeon, ^bSeoul St. Mary's Hospital, The Catholic University of Korea, Republic of Korea, ^cSiemens Healthcare, Seoul, Korea, ^dSiemens Healthcare, Erlangen, Germany.

*Correspondence: Sung Hun Kim, Department of Radiology, Seoul St. Mary's Hospital, College of Medicine, The Catholic University of Korea, 505 Banpo-dong, Seocho-Gu, Seoul 137-701, Republic of Korea (e-mail: rad-ksh@catholic.ac.kr).

Copyright © 2021 the Author(s). Published by Wolters Kluwer Health, Inc. This is an open access article distributed under the terms of the Creative Commons Attribution-Non Commercial License 4.0 (CCBY-NC), where it is permissible to download, share, remix, transform, and buildup the work provided it is properly cited. The work cannot be used commercially without permission from the journal.

How to cite this article: Lee YJ, Kim SH, Kang BJ, Son YH, Grimm R. Associations between angiogenic factors and intravoxel incoherent motion (IVIM)-derived parameters in diffusion-weighted magnetic resonance imaging of breast cancer. *Medicine* 2021;100:41(e27495).

Received: 8 February 2021 / Received in final form: 11 August 2021 / Accepted: 23 September 2021

<http://dx.doi.org/10.1097/MD.0000000000027495>

1. Introduction

Breast cancer is the most frequently diagnosed cancer in women worldwide. Owing to its strong invasiveness and metastasis ability, breast cancer is the leading cause of cancer-related deaths among women.^[1,2] Angiogenesis is a well-known critical factor that stimulates tumor growth and the development of metastases.^[3–5] Microvascular density (MVD) and vascular endothelial growth factor (VEGF) status are commonly used as angiogenic markers and have been proven to be the prognostic factors associated with treatment response and the relapse-free and overall survival of cancer patients.^[6–8]

Diffusion-weighted imaging (DWI) has been extensively explored in oncologic imaging. Most such studies have relied on the apparent diffusion coefficient (ADC), a robust and easy-to-calculate parameter.^[9] To date, many studies have attempted to demonstrate a correlation between ADC and angiogenic markers; however, these studies yielded variable results, which range from no correlation in head and neck cancer^[10] to a positive correlation in cervical and pancreatic cancer.^[11] Intravoxel incoherent motion (IVIM), an advanced DWI technique, has received increased interest because it can be used to estimate perfusion-related parameters, including pseudodiffusivity (D^*), which is indicative of blood flow, and the perfusion fraction (f), which is indicative of the fractional volume of active capillaries in a tumor.^[12,13] We hypothesized that IVIM may be more sensitive

for predicting angiogenic markers. Moreover, IVIM can provide perfusion-related parameters without the need for contrast agents, which is important, considering the recent finding of gadolinium deposition in the brain after repeated contrast injections.^[14] If MVD and VEGF can be evaluated using IVIM, then IVIM could become a noninvasive tool to monitor the effects of vascular targeting agents in the routine follow-up of cancer patients.

However, IVIM values are computed with multistep post-processing, based on the fitting algorithm used, and limited interalgorithm agreement and quantification of vascular diffusion effects impose a significant challenge.^[15–18] In addition, previous IVIM algorithm studies have used a single section of a tumor as a representation of the whole tumor by contouring the tumor or placing regions-of-interest on one representative section of the tumor. However, considering the heterogeneity of tumors, the subjective choice of the measurement section by a researcher may result in measurement deviations.^[19] More sophisticated methods such as histogram analysis have recently been applied to these maps and have yielded additional biomarkers and more information in patients with breast cancer.^[20] Therefore, we investigated the associations between MVD, VEGF, and IVIM MRI parameters, using 4 different curve-fitting algorithms and whole-tumor histogram analysis in patients with invasive breast carcinomas.

2. Materials and methods

This retrospective study was approved by the ethics committee of our hospital (IRB KC19RESI0706), and the requirement for obtaining informed patient consent was waived owing to the nature of the study.

2.1. Patients and IVIM acquisition

Seventy-eight patients with invasive breast carcinomas, which were diagnosed between 2014 and 2016, were considered for enrollment in our study, based on the following criteria: invasive ductal carcinoma was confirmed by percutaneous biopsy and IVIM DWI with 10 b values on a 3-T system were acquired for the preoperative evaluation. Exclusion criteria were a lack of consent by the patient for immunohistochemical staining (n = 10), failure of the acquisition of IVIM parameters because of artifact (n = 2), systemic therapy with distant metastasis (n = 3), neoadjuvant chemotherapy (n = 8). Fifty-five patients were included in the analysis of the IVIM parameters and angiogenic markers. All patients included in this study underwent surgery. Histopathologic information was obtained from the pathology reports in the patients' medical records. For each patient, the single largest lesion located in the breast on one side was selected.

For the IVIM sequence, the patients were examined in a 3.0-T MRI imaging system (Magnetom Verio; Siemens Healthcare, Erlangen, Germany) with a dedicated bilateral breast surface coil. The patients were placed in the prone position. IVIM was obtained with single-shot echo-planar imaging, using 10 b values (0 s/mm², 25 s/mm², 50 s/mm², 75 s/mm², 100 s/mm², 150 s/mm², 200 s/mm², 300 s/mm², 500 s/mm², and 800 s/mm²) with the following parameters: repetition time/echo time, 5600/5.5 ms; field of view, 340 mm × 170 mm; matrix size, 192 × 192; slice thickness, 4 mm; and acquisition time, approximately 4 minutes.

2.2. IVIM analysis and four fitting algorithms for IVIM-derived parameters

The IVIM data were retrospectively evaluated with consensus of 2 radiologists with >15 years and 5 years of experience, respectively, in breast MRI. DICOM images from the IVIM sequence were postprocessed using the prototype software MR Body Diffusion Toolbox, v1.3.3 (Siemens Healthcare) to extract the ADC and IVIM parameters. In the IVIM model, the relationship between signal variation and b factor is expressed as

$$S_b/S_0 = (1 - f) \times \exp(-b \cdot D) + f \times \exp(-b \cdot D^*)$$

where S is the signal intensity; f is the perfusion fraction representing the volume fraction of microcirculation; D^* is the pseudodiffusion coefficient related to perfusion-related diffusion; and D is the true diffusion coefficient that reflects the pure molecular diffusion.

In this study, we proposed 4 curve-fitting algorithms for IVIM analysis. Algorithm 1 involves linear regression to determine D and f from high b values, and linear regression to determine D^* from low b values, as proposed in method 3 by Suo et al.^[15] Algorithm 2 involves linear regression to determine D and f from high b values, and nonlinear fitting to determine D^* from low b values, as proposed by Sigmund et al.^[21] Algorithm 3 involves linear regression to determine D and f from high b values (by neglecting D^* effects), and linear regression to determine D^* from b values ≤ 50 s/mm² (by neglecting D effects). Algorithm 4 involves full nonlinear fitting, based on the Nelder–Mead simplex optimization technique.

The prototype software MR Multiparametric Analysis, v 1.0.0 (Siemens Healthcare), was used for histogram analysis on a personal computer running Windows (Microsoft Corporation, Redmond, WA). The radiologist manually marked the seed points for the target tumor on axial and multiplanar reconstruction images and then ran the segmentation (Fig. 1). The results of segmentation could be corrected by adjusting the seed points. Finally, voxel-based histogram data were generated for the whole tumor volume, and the following parameters were calculated: the 10th percentile, 25th percentile, 50th percentile (ie, median), mean, 75th percentile, 90th percentile, skewness (describes asymmetry), and kurtosis (describes peakedness).

2.3. Pathologic analysis

Tumor angiogenesis was evaluated based on MVD and VEGF expression. A pathologist with 15 years of experience in oncologic pathology, analyzed immunohistochemical staining for CD34 (clone QB End 10, 1:100; DAKO, Carpinteria, CA) and VEGF (clone A-20, 1:200; Santa Cruz, Heidelberg, Germany). Any positively stained endothelial cells that were separate from adjacent microvessels or tumor cells were considered to be countable vessels. CD34-immunostained sections were examined under a microscope at 40-magnification for the area containing the greatest number of microvessels. Five high-power fields were manually counted, and the average counts of the 5 fields were recorded. As previous methods have shown,^[22] VEGF immunostaining was assessed using the scoring system, which is based on the percentage of positive tumor cells (0, 0% immunopositive cells; 1, <25% positive cells; 2, 26%–50% positive cells; 3, >50% positive cells; 4, 67%–100% positive cells) and staining intensity (0, negative; 1, weak; 2, moderate; and 3, strong). In terms of the level of VEGF expression, 2 groups were classified (ie, low vs high VEGF expression).

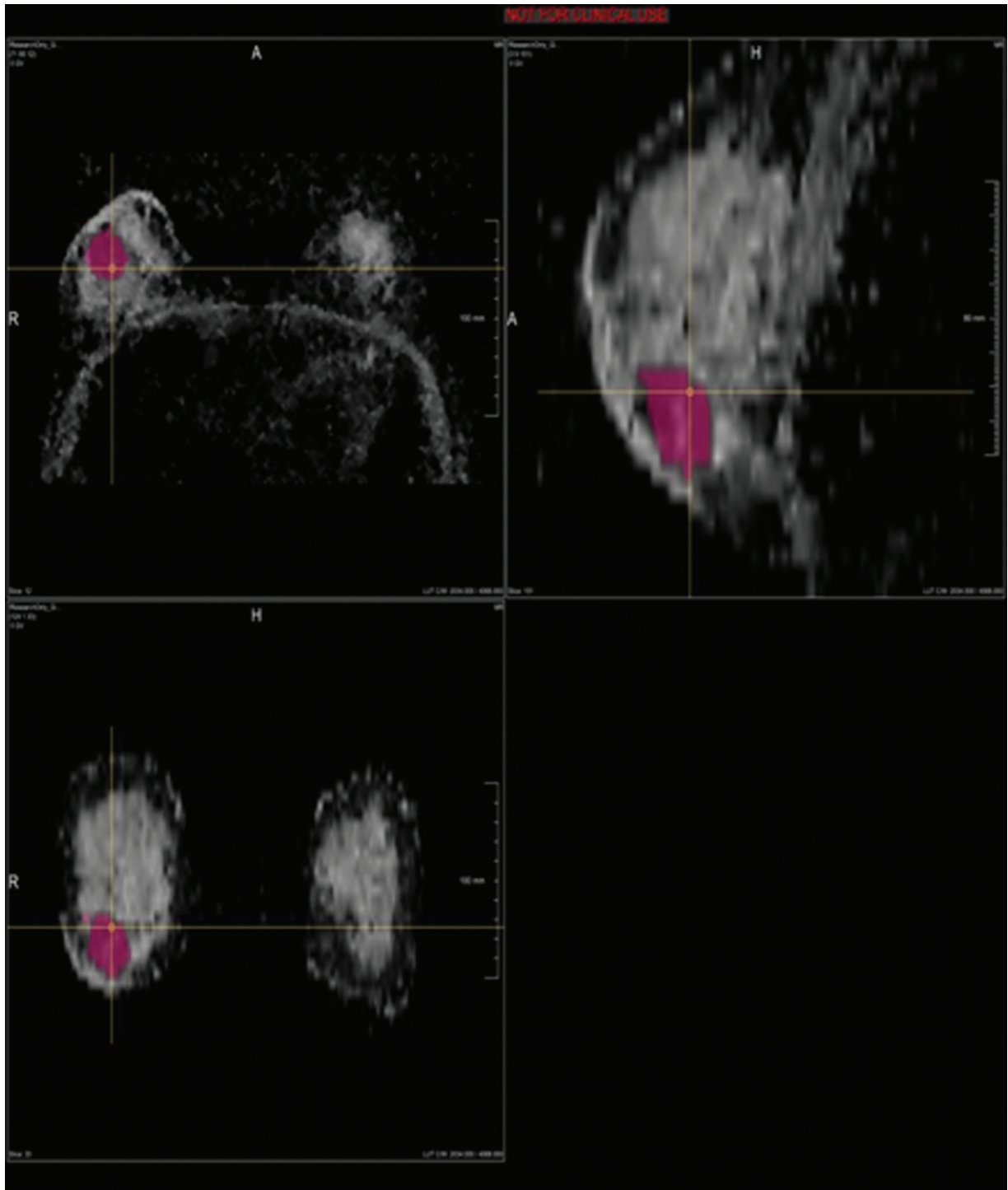


Figure 1. MR images of a 52-year-old woman with a 3.3-cm surgically verified right invasive ductal breast cancer and high vascular endothelial growth factor (VEGF) expression. (A) Regions of interest were manually traced along the margin of the cancer on axial and multiplanar reconstruction images. (B–D) The D^* (B), D (C), and f (D) parameter maps calculated from each of the four curve-fitting algorithms are displayed with histograms for the whole tumor. The values, obtained using algorithm 3, are as follows: D^*_{10} $113 \times 10^{-4} \text{ mm}^2/\text{s}$, D^*_{25} $201 \times 10^{-4} \text{ mm}^2/\text{s}$, D^*_{median} $267 \times 10^{-4} \text{ mm}^2/\text{s}$, D^*_{mean} $270 \times 10^{-4} \text{ mm}^2/\text{s}$, D^*_{75} $334 \times 10^{-4} \text{ mm}^2/\text{s}$, D^*_{90} $416 \times 10^{-4} \text{ mm}^2/\text{s}$, f_{10} 58%, f_{25} 76%.

2.4. Statistical analysis

All statistical analyses were conducted using the SAS Enterprise Guide 5.1 software package (SAS Institute, Cary, NC), SPSS software (version 26.0; SPSS, Inc., Chicago, IL) IBM SPSS Statistics Grad Pack 26.0. P values $< .05$ were considered to be statistically significant. Intraclass correlation coefficient (ICC) and analysis of

variance (ANOVA) were calculated to assess the agreements between IVIM parameters derived using the different fitting algorithms. ICC values close to 1 indicated good interalgorithm reliability. We calculated the precision of the parameter estimates by means of their coefficients of variation (CVs).^[23,24] Spearman correlation was applied to determine the association between

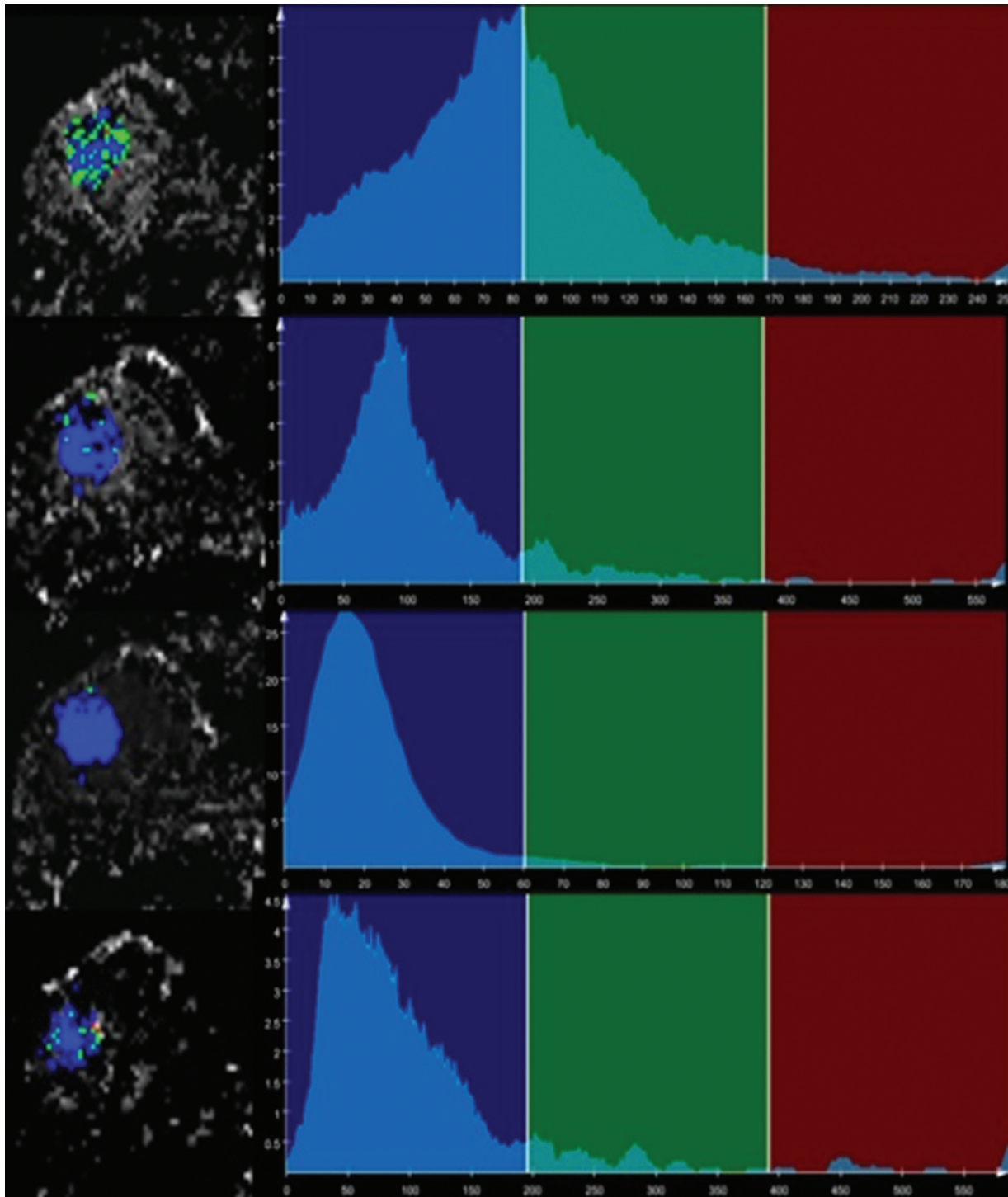


Figure 1. (Continued)

IVIM-derived parameters and MVD. Differences in IVIM-derived parameters between the low and high expression of VEGF were calculated using the Mann–Whitney U test.

3. Results

3.1. Histopathological characteristics

The mean tumor size of 55 invasive breast cancers was 2.5 ± 0.9 cm (range, 1.1–5.4 cm). The mean patient age was 52.6 ± 10.7

years (range, 36–74 years). The mean MVD was 41.2 ± 18.4 . VEGF expression was low in 29.1% (16/55) of the tumors and high in 70.9% (39/55) of the tumors.

3.2. Interalgorithm agreement between IVIM-derived parameters

Table 1 presents the histogram analysis of each D^* value, calculated from the four different algorithms, and the results of

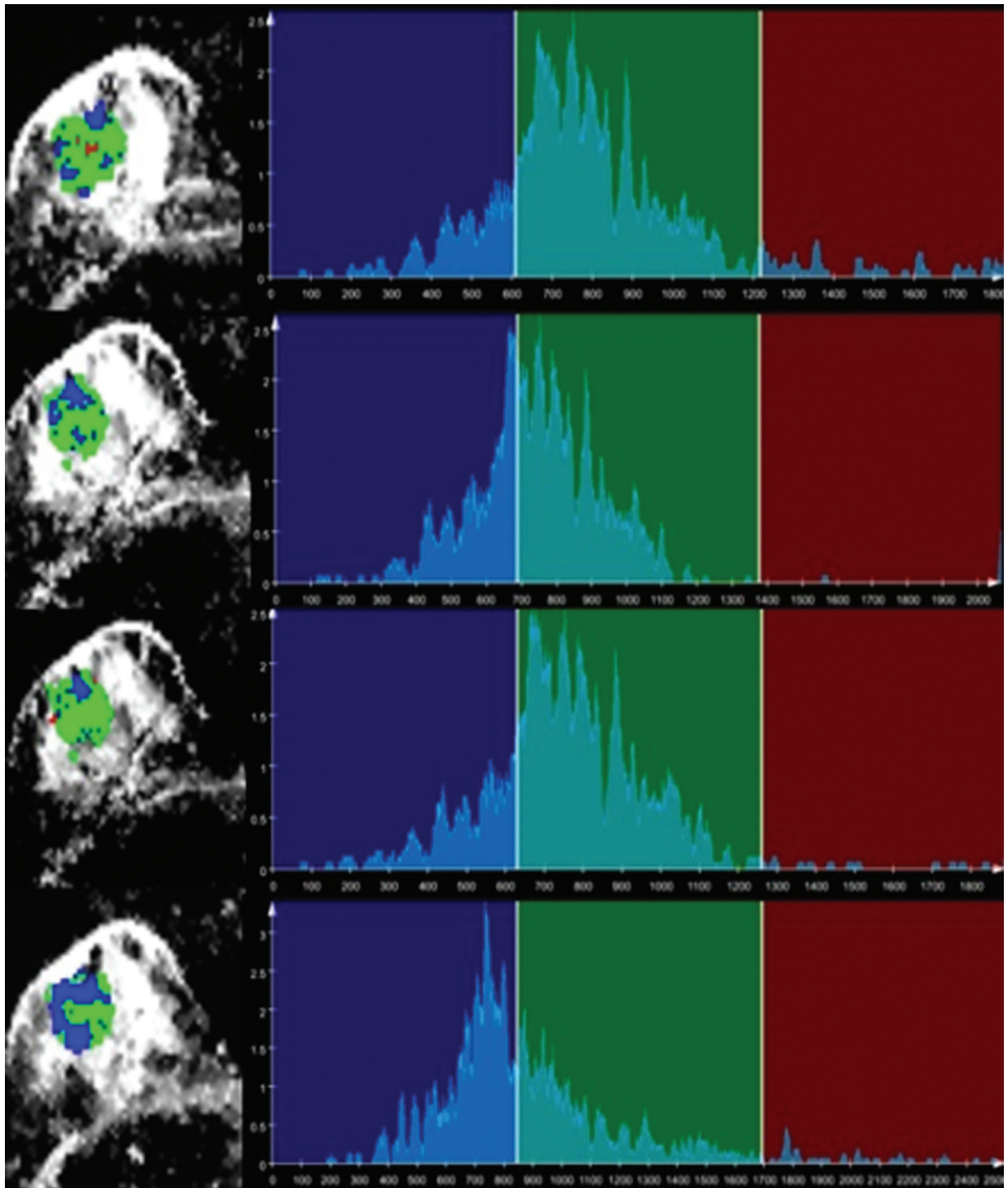


Figure 1. (Continued)

the ANOVA. Significant difference ($P < .001$) was observed for all D^* parameters calculated from each algorithm. All f parameters, except for the 10th percentile, skewness, and kurtosis, also showed significant differences among the algorithms ($P < .005$). However, all D values calculated from each of the 4 algorithms, except for the 10th and 25th percentiles and skewness values, revealed no significant difference ($P > .005$).

With regard to the ICC test for interalgorithm agreement of IVIM-derived parameters calculated from the four algorithms, all D^* values also showed poor to slight agreement ($ICC < 0.1$), which was similar to the results obtained with ANOVA. Examples of IVIM-derived parameter maps of breast cancer derived by the 4 algorithms are shown in Figures 1 and 2.

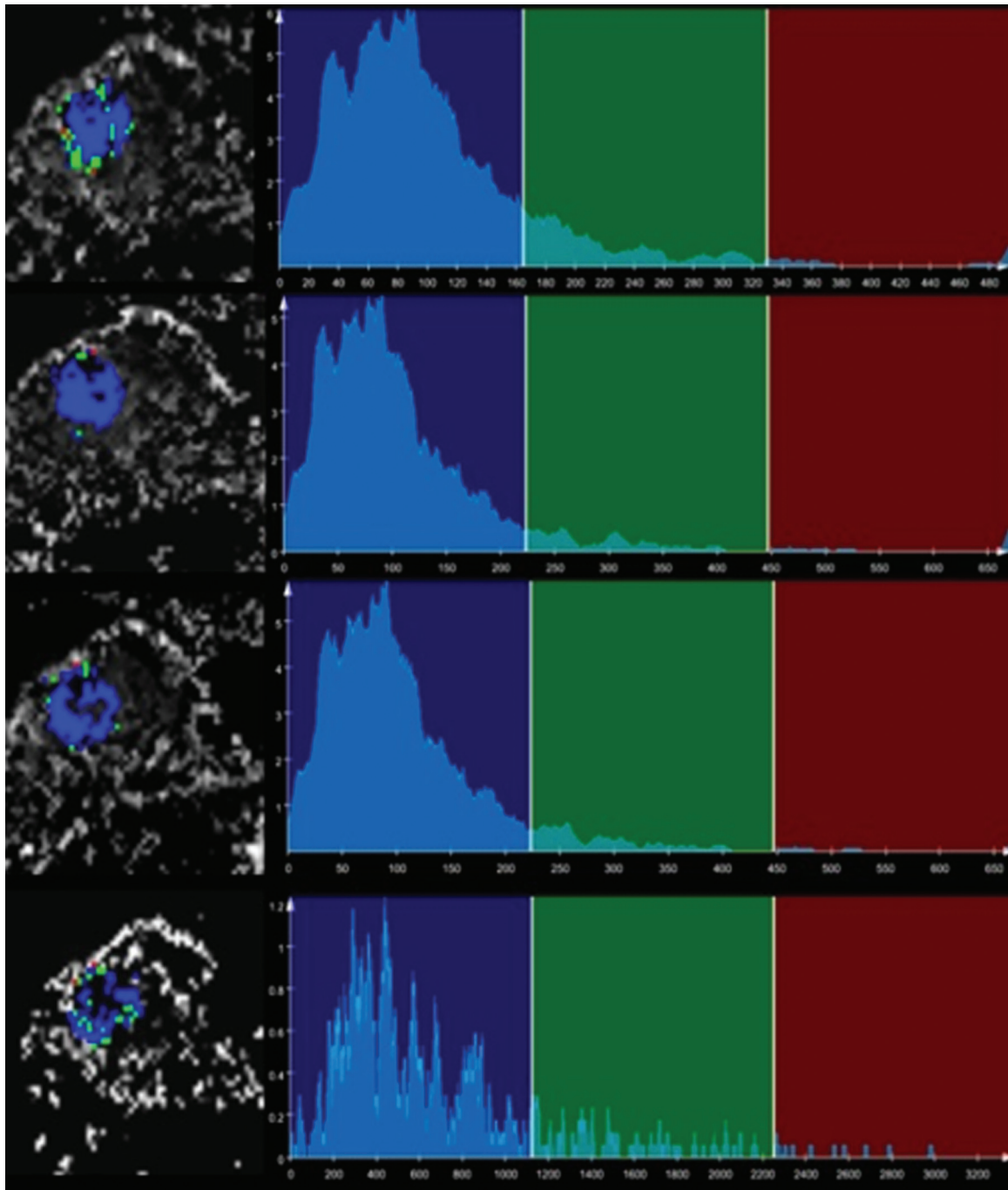


Figure 1. (Continued).

3.3. IVIM-derived parameter precision

We assessed the quality of an IVIM-derived parameter using the CV as the quantitative precision measure. Figure 3 shows the bar plots of the CVs for the IVIM-derived parameters calculated from the 4 different algorithms. The CV of D^* calculated from algorithm 4 (22%) was lower than that obtained from algorithms 1 (24.8%), 2 (27.3%), and 3 (40.9%). The CV calculated from algorithm 4 (33.9%) was also lower than that obtained from algorithms 1 (39.6%), 2 (44.7%), and 3 (48.4%).

3.4. Correlations between IVIM-derived parameters and tumor angiogenesis

In Table 2, lower D^*_{10} , D^*_{25} , D^*_{50} , D^*_{mean} , D^*_{75} , D^*_{90} , f_{10} , and f_{25} values, obtained using algorithm 3, and D^*_{90} values, obtained using algorithm 2, were significantly associated with low VEGF expression ($P < .05$). However, the other IVIM-derived parameters, which were obtained using curve-fitting algorithm 1, 2, and 4, showed no statistically significant correlation with VEGF expression. With regard to MVD, we

Table 1
Interalgorithm agreement of D* parameters with histogram analysis.

	IVIM D* (10 ⁻⁴ mm ² /s) parameter				P
	Algorithm 1	Algorithm 2	Algorithm 3	Algorithm 4	
10 th percentile					<.0001
Mean ±SD	27.7 ±13	31.3 ±21.2	8.9 ±2.7	48.3 ±49.4	
Median (IQR)	26.5 (18.5–34.5)	23.5 (17.5–40.5)	8.5 (7–10.5)	39 (0–70.2)	
25 th percentile					<.0001
Mean ±SD	52.4 ±19.5	63.8 ±26.4	16.2 ±4.8	134.7 ±74.9	
Median (IQR)	50 (40–62.5)	59.5 (45.5–74.5)	15.5 (12.5–19.5)	130.5 (80–209)	
50 th percentile					<.0001
Mean ±SD	86.8 ±25.9	106.3 ±32	27.9 ±11	238.5 ±60.7	
Median (IQR)	78.5 (70–94.5)	100.5 (87.5–117.5)	24.5 (20.5–32.5)	238 (203.5–278)	
Mean					<.0001
Mean ±SD	94.2 ±23.3	123.6 ±33.8	34.9 ±14.3	251.3 ±55.3	
Median (IQR)	88.9 (81–99.2)	117.3 (103.7–134.5)	31.5 (23.3–43.1)	249.9 (214.1–290.3)	
75 th percentile					<.0001
Mean ±SD	126.6 ±31.5	160.1 ±43.3	45 ±20.9	339.5 ±69.2	
Median (IQR)	119.5 (105.5–133)	152.5 (133.5–179.5)	40 (29.5–53.5)	334 (291–386)	
90 th percentile					<.0001
Mean ±SD	170.3 ±38.2	234.8 ±70.5	68.8 ±34.5	461.2 ±103.7	
Median (IQR)	158.5 (143–188)	217.5 (196.5–261.5)	62.5 (41.5–87.5)	436 (400–505.6)	
Skewness					<.0001
Mean ±SD	0.9 ±0.5	1.6 ±0.8	2.3 ±1.2	0.7 ±0.4	
Median (IQR)	0.8 (0.6–1.2)	1.5 (1.1–2.1)	2 (1.6–3)	0.7 (0.5–1)	
Kurtosis					<.0001
Mean ±SD	1.6 ±2.4	4.9 ±5.5	10.6 ±13.5	1.1 ±1	
Median (IQR)	0.9 (0.1–2.1)	3.5 (1.6–7.5)	6.3 (2.8–14.8)	0.9 (0.4–1.5)	

Data in parentheses are the interquartile range (IQR). The P values were calculated using analysis of variance. IVIM=intravoxel incoherent motion, SD=standard deviation.

did not find statistically significant correlations with IVIM-derived parameters, calculated from the four different algorithms (P > .05).

4. Discussion

In this study, we investigated the relationship between MVD, VEGF, and IVIM-derived parameters, obtained by 4 curve-fitting algorithms, in patients with invasive breast cancers. We found significant associations between VEGF expression and perfusion-related IVIM parameters, which were obtained using curve-fitting algorithm 3, in invasive breast cancer. In our histogram analysis, higher D*₁₀, D*₂₅, D*_{median}, D*_{mean}, D*₇₅, D*₉₀, f₁₀, and f₂₅ values, calculated using fitting algorithm 3, were associated with high VEGF expression. IVIM may aid in the evaluation of treatment response to VEGF-targeted therapy in breast cancer. Previous studies have reported this finding. For example, in a murine embryonal rhabdomyosarcoma model, Yuan et al^[25] also showed a positive correlation between the D* value and VEGF expression. Togao et al^[26] exhibited excellent agreement between the f value and the histological vascular density in meningiomas. Klau et al^[27] reported a good correlation between MVD and IVIM perfusion parameters in pancreatic cancer. However, some reports indicate that IVIM may not be sensitive in this regard. In the study by Yang et al^[28] using a hepatocellular carcinoma mouse model, MVD was not correlated with IVIM perfusion parameters. We also failed to reveal any significant association between IVIM-derived parameters and MVD. The correlation between IVIM parameters and microvascular histology is not entirely clear. Further studies are needed to validate the correlation.

We evaluated whole-tumor histograms to assess interalgorithm agreements between IVIM-derived parameters calculated using four different curve-fitting algorithms in breast cancer. In this study, D* histogram parameters differed significantly, depending on which of the four algorithms was used, whereas the 50th, 75th, and 90th percentiles, mean, and kurtosis of the D parameters revealed no significant interalgorithm differences. Barbieri et al^[16] used 6 calculation methods for an IVIM model in upper abdominal organs and showed that the variability of D* value was higher than that of f values, which was higher than the variability of D values. Suo et al^[15] also showed significant differences for each IVIM-derived parameter obtained using 3 different methods in 30 patients with breast cancer. This finding was in accordance with that of existing reports.^[17,18] However, in their studies, the authors measured the mean pixel value within a single-slice map, which did not encompass the entire tumor volume. By contrast, our histogram analysis showed heterogeneous intratumoral signal intensity and the whole tumor volume. Other histogram analysis by Song et al^[29] obtained similar results in that their histogram parameters, derived from true diffusion coefficient maps, were more reproducible than those derived from pseudodiffusion coefficients and perfusion fraction maps. However, they investigated rat breast carcinomas and did not assess interalgorithm agreement in vivo.

By means of the CV in our IVIM data, D had higher precision than did D* or f. This result was consistent with reports by Freiman et al.^[23] The IVIM-derived parameter, f represents an “incoherently flowing” blood volume, whereas D* is related to blood speed. D* is primarily determined at the range of lower b values (typically < 100 s/mm²), so multiple data sampling in the lower b value range and an higher signal-to-noise ratio than is available with most clinical DWI

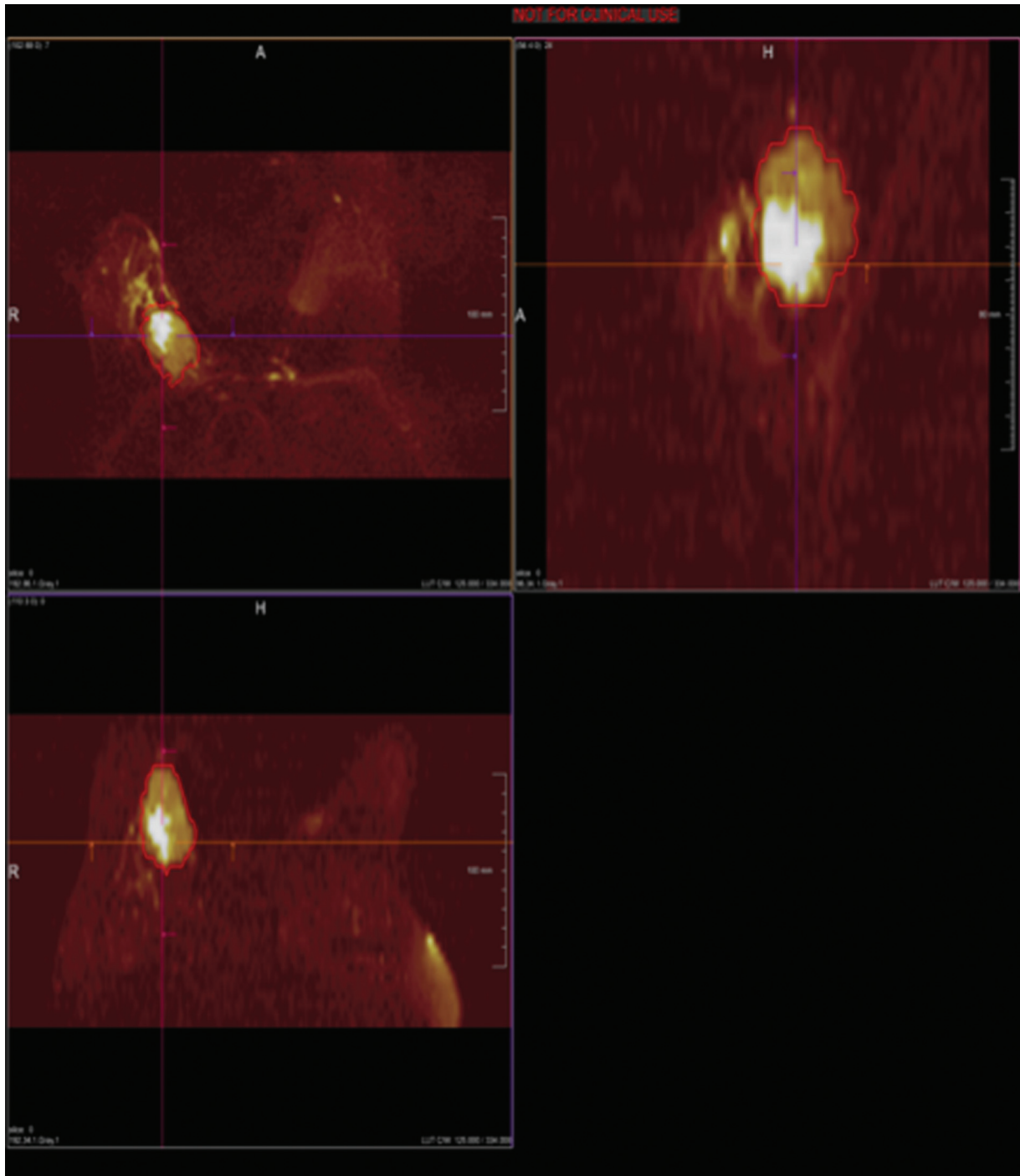


Figure 2. MR images of a 67-year-old woman with a 4.5-cm surgically verified right invasive ductal breast cancer and low vascular endothelial growth factor (VEGF) expression. (A) Regions of interest were drawn along the tumor boundary on axial and multiplanar reconstruction images. (b-d) The D^* (B), D (C), and f (D) parameter maps calculated from each of the four curve-fitting algorithms are displayed with histograms for the entire tumor. The values, obtained using algorithm 3, are as follows: $D_{10}^* 39 \times 10^{-4} \text{ mm}^2/\text{s}$, $D_{25}^* 116 \times 10^{-4} \text{ mm}^2/\text{s}$, $D_{\text{median}}^* 226 \times 10^{-4} \text{ mm}^2/\text{s}$, $D_{\text{mean}}^* 227 \times 10^{-4} \text{ mm}^2/\text{s}$, $D_{75}^* 319 \times 10^{-4} \text{ mm}^2/\text{s}$, $D_{90}^* 410 \times 10^{-4} \text{ mm}^2/\text{s}$, $f_{10} 27\%$, $f_{25} 54\%$.

methods, are needed for the precise estimation of D^* , as shown by Pekar et al.^[30] Many different curve-fitting algorithms have been developed to obtain more reliable estimates of perfusion-related IVIM parameters. Thus, the variations between IVIM-derived parameters from different algorithms may be the natural consequence of the complex mathematical approaches. In addition,

IVIM is sensitive to any fluid flow. Besides microcapillary perfusion, active transport, resulting from secretion of the breast ducts, may be explored in the breast.

We found good results with D^* parameters obtained using algorithm 3. However, some limitations in this study should be noted. First, our study was retrospective. Also, we were unable to

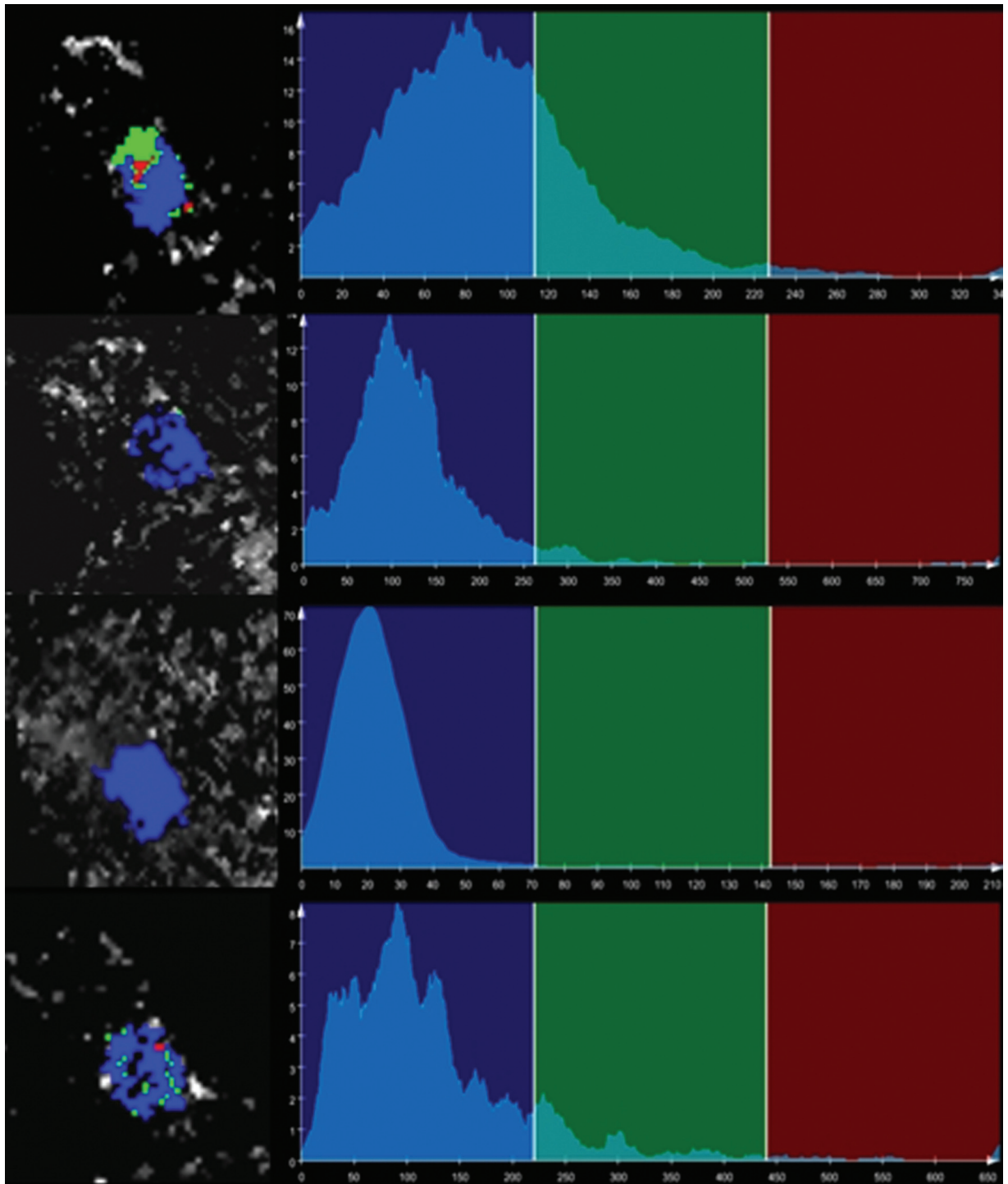


Figure 2. (Continued)

evaluate optimized b-value selection for biexponential IVIM analysis. Previous literatures have shown that the choice of b-values affects IVIM-derived parameter calculation.^[13] Lastly, the sample size was small. Larger, prospective studies may be needed for a further investigation to validate the correlation of IVIM parameters and angiogenic factors.

In conclusion, the D^* and f IVIM parameters, obtained using curve-fitting algorithm 3, were significantly correlated with VEGF expression in breast cancer. Thus, IVIM may be used as a noninvasive tool to reflect VEGF expression. Perfusion-related IVIM parameters should be more widely investigated in clinical studies in the future.

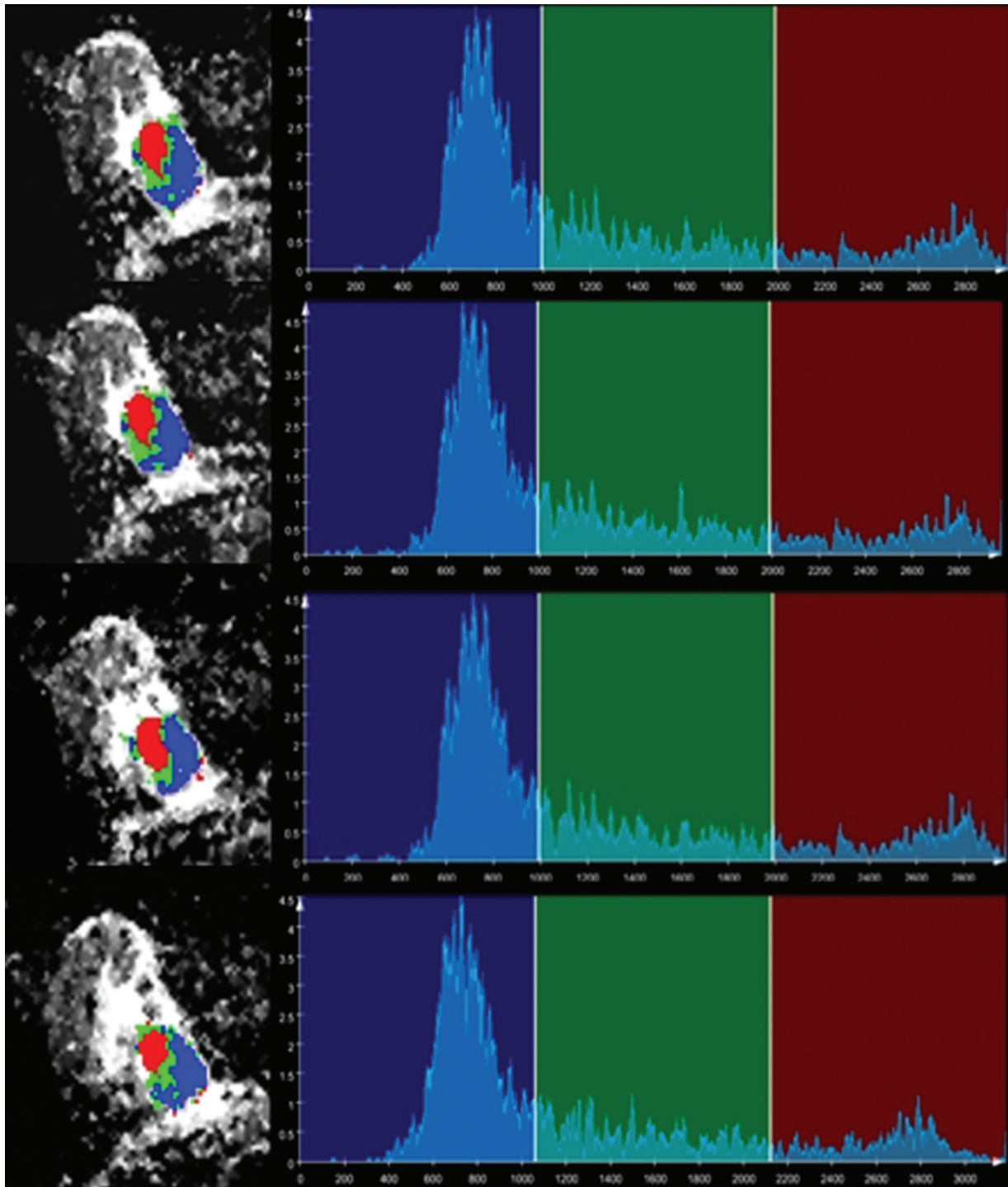


Figure 2. (Continued)

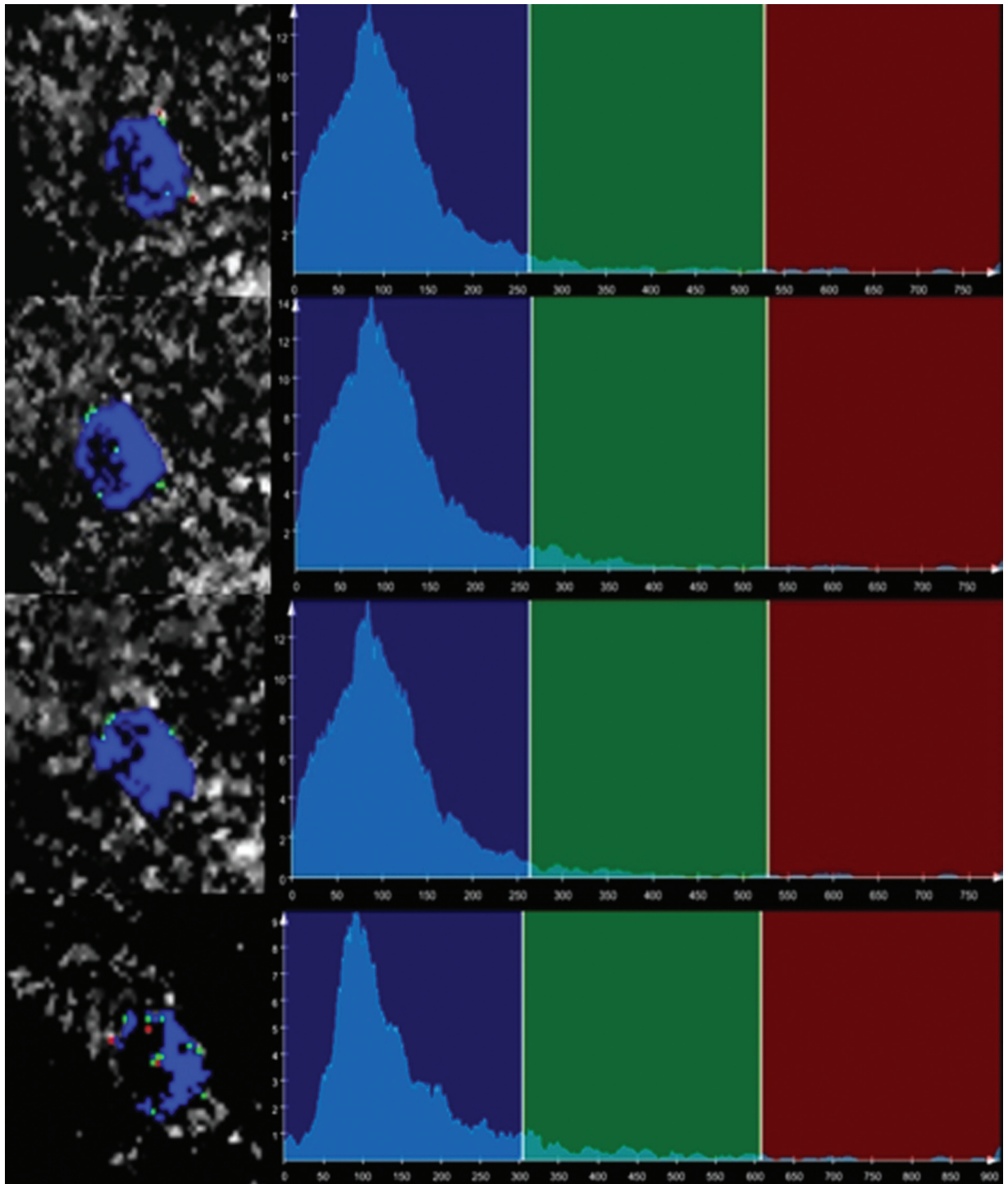


Figure 2. (Continued).

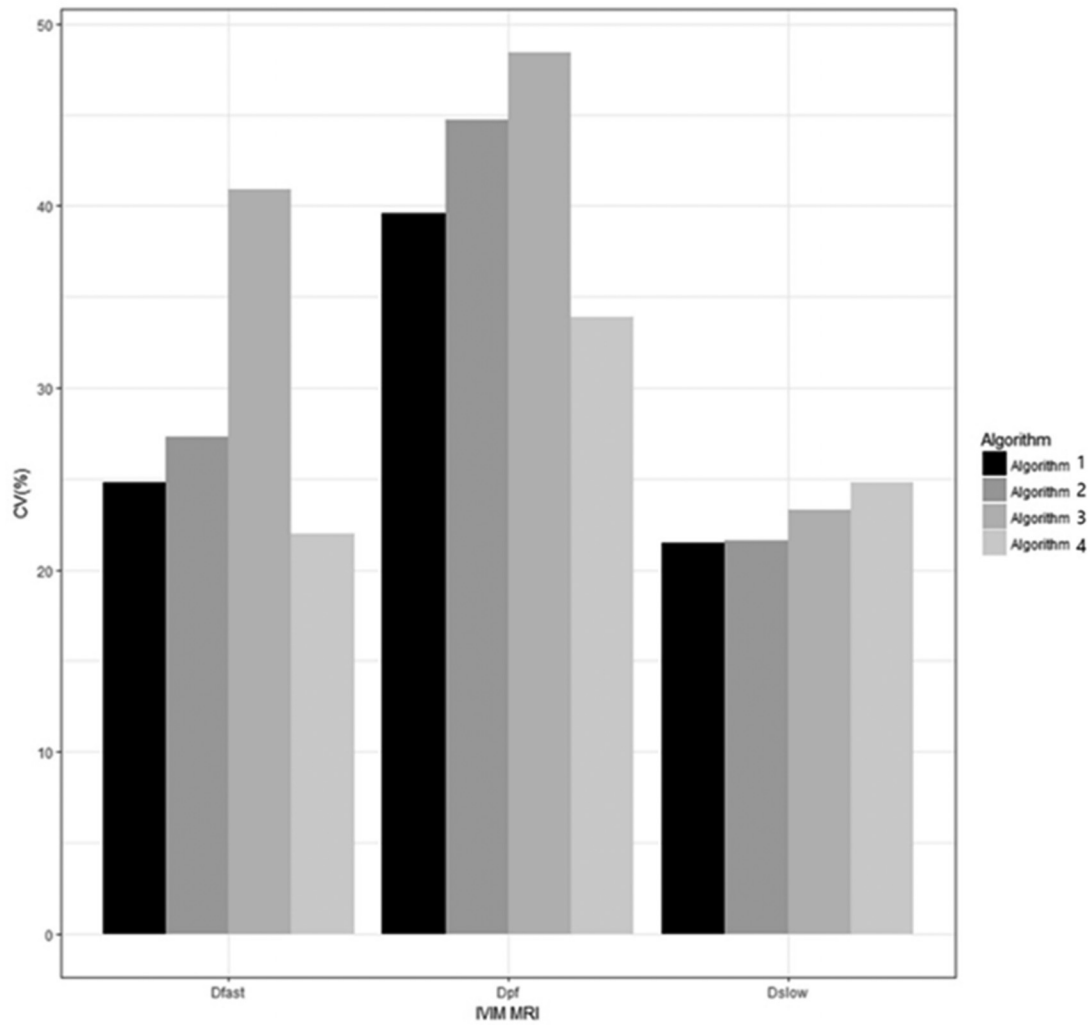


Figure 3. The bar graphs of the coefficients of variance for the intravoxel incoherent motion parameters obtained using four different curve-fitting algorithms.

Table 2
Summary of correlation analysis between intravoxel incoherent motion parameters and VEGF expression.

IVIM curve-fitting algorithm	IVIM-derived parameter	Low VEGF expression	High VEGF expression	P
Algorithm 3	D ₁₀ [*]	8.27 (10 ⁻⁴ mm ² /sec)	9.78 (10 ⁻⁴ mm ² /s)	.043
	D ₂₅ [*]	15.01	17.84	.012
	D ₅₀ [*]	25.22	31.25	.019
	D _{mean} [*]	31.44	40.62	.024
	D ₇₅ [*]	40.03	51.97	.044
	D ₉₀ [*]	61.42	82.16	.041
Algorithm 3	f ₁₀	35.19 (%)	44.09 (%)	.010
	f ₂₅	68.67	86.47	.005
Algorithm 2	D ₉₀ [*]	220.45 (10 ⁻⁴ mm ² /s)	275.03 (10 ⁻⁴ mm ² /s)	.031

IVIM = intravoxel incoherent motion, VEGF = vascular endothelial growth factor.

Author contributions

Conceptualization: Sung Hun Kim
Data curation: Youn Joo Lee, Bong Joo Kang, Sung Hun Kim.
Formal analysis: Youn Joo Lee, Yo Han Son.
Investigation: Youn Joo Lee
Methodology: Yo Han Son, Sung Hun Kim

Project administration: Sung Hun Kim.
Software: Yo Han Son, Robert Grimm.
Supervision: Sung Hun Kim
Validation: Bong Joo Kang
Writing – original draft: Youn Joo Lee.
Writing – review & editing: Sung Hun Kim, Robert Grimm

References

- [1] Bray F, Ferlay J, Soerjomataram I, Siegel RL, Torre LA, Jemal A. Global cancer statistics 2018: GLOBOCAN estimates of incidence and mortality worldwide for 36 cancers in 185 countries. *CA Cancer J Clin* 2018; 68:394–424.
- [2] Ghislain I, Zikos E, Coens C, et al. Health-related quality of life in locally advanced and metastatic breast cancer: methodological and clinical issues in randomised controlled trials. *Lancet Oncol* 2016;17:e294–304.
- [3] Hanahan D, Weinberg RA. Hallmarks of cancer: the next generation. *Cell* 2011;144:646–74.
- [4] Folkman J. Role of angiogenesis in tumor growth and metastasis. *Semin Oncol* 2002;29:15–8.
- [5] Weidner N, Semple JP, Welch WR, Folkman J. Tumor angiogenesis and metastasis—correlation in invasive breast carcinoma. *N Engl J Med* 1991;324:1–8.
- [6] Choi WW, Lewis MM, Lawson D, Yin-Goen Q, Birdsong GG, Cotsonis GA. Angiogenic and lymphangiogenic microvessel density in breast carcinoma: correlation with clinicopathologic parameters and VEGF-family gene expression. *Mod Pathol* 2005;18:143–52.
- [7] Bevilacqua P, Barbareschi M, Verderio P, Boracchi P, Caffo O, Dalla Palma P. Prognostic value of intratumoral microvessel density, a measure of tumor angiogenesis, in node-negative breast carcinoma—results of a multiparametric study. *Breast Cancer Res Treat* 1995;36:205–17.
- [8] Gasparini G. Prognostic value of vascular endothelial growth factor in breast cancer. *Oncologist* 2000;5:37–44.
- [9] Xu F, Liang Y, Guo Y, Liang ZP, Wu M, Chen S. Diagnostic performance of whole-lesion apparent diffusion coefficient histogram analysis metrics for differentiating benign and malignant breast lesions: a systematic review and diagnostic meta-analysis. *Acta Radiol* 2020; 61:1165–75.
- [10] Meyer HJ, Hamerla G, Leifels L, Höhn AK, Surov A. Whole-lesion ADC histogram analysis is not able to reflect microvessel density in HNSCC. *Medicine (Baltimore)* 2019;98:e15520.
- [11] Meyer HJ, Wienke A, Surov A. Association between VEGF expression and diffusion weighted imaging in several tumors—a systematic review and meta-analysis. *Diagnostics* 2019;9:126.
- [12] Le Bihan D, Breton E, Lallemand D, Aubin ML, Vignaud J, Laval-Jeantet M. Separation of diffusion and perfusion in intravoxel incoherent motion MR imaging. *Radiology* 1988;168:497–505.
- [13] Iima M, Le Bihan D. Clinical intravoxel incoherent motion and diffusion MR imaging: past, present, and future. *Radiology* 2016;278:13–32.
- [14] Gulani V, Calamante F, Shellock FG, Kanal E, Reeder SB. Gadolinium deposition in the brain: summary of evidence and recommendations. *Lancet Neurol* 2017;16:564–70.
- [15] Suo S, Lin N, Wang H, et al. Intravoxel incoherent motion diffusion-weighted MR imaging of breast cancer at 3.0 tesla: comparison of different curve-fitting methods. *J Magn Reson Imaging* 2015;42:362–70.
- [16] Barbieri S, Donati OF, Froehlich JM, Thoeny HC. Impact of the calculation algorithm on biexponential fitting of diffusion-weighted MRI in upper abdominal organs. *Magn Reson Med* 2016;75:2175–84.
- [17] Park HJ, Sung YS, Lee SS, et al. Intravoxel incoherent motion diffusion-weighted MRI of the abdomen: The effect of fitting algorithms on the accuracy and reliability of the parameters. *J Magn Reson Imaging* 2017;45:1637–47.
- [18] Gurney-Champion OJ, Klaassen R, Froeling M, et al. Comparison of six fit algorithms for the intra-voxel incoherent motion model of diffusion-weighted magnetic resonance imaging data of pancreatic cancer patients. *PLoS One* 2018;13:e0194590.
- [19] Lee HJ, Rha SY, Chung YE, et al. Tumor perfusion-related parameter of diffusion-weighted magnetic resonance imaging: correlation with histological microvessel density. *Magn Reson Med* 2014; 71:1554–8.
- [20] Cho GY, Moy L, Kim SG, et al. Evaluation of breast cancer using intravoxel incoherent motion (IVIM) histogram analysis: comparison with malignant status, histological subtype, and molecular prognostic factors. *Eur Radiol* 2016;26:2547–58.
- [21] Sigmund EE, Cho GY, Kim S, et al. Intravoxel incoherent motion imaging of tumor microenvironment in locally advanced breast cancer. *Magn Reson Med* 2011;65:1437–47.
- [22] Li Y, Wei X, Zhang S, Zhang J. Prognosis of invasive breast cancer after adjuvant therapy evaluated with VEGF microvessel density and microvascular imaging. *Tumour Biol* 2015;36:8755–60.
- [23] Freiman M, Perez-Rossello JM, Callahan MJ, et al. Reliable estimation of incoherent motion parametric maps from diffusion-weighted MRI using fusion bootstrap moves. *Med Image Anal* 2013;17:325–36.
- [24] Bogner W, Gruber S, Pinker K, et al. Diffusion-weighted MR for differentiation of breast lesions at 3.0T: how does selection of diffusion protocols affect diagnosis? *Radiology* 2009;253:341–51.
- [25] Yuan Y, Zeng D, Zhang Y, et al. Intravoxel incoherent motion diffusion-weighted imaging assessment of microvascular characteristics in the murine embryonal rhabdomyosarcoma model. *Acta Radiol* 2020;61: 260–6.
- [26] Togao O, Hiwatashi A, Yamashita K, et al. Measurement of the perfusion fraction in brain tumors with intravoxel incoherent motion MR imaging: validation with histopathological vascular density in meningiomas. *Br J Radiol* 2018;91:20170912.
- [27] Klau M, Mayer P, Bergmann F, et al. Correlation of histological vessel characteristics and diffusion-weighted imaging intravoxel incoherent motion-derived parameters in pancreatic ductal adenocarcinomas and pancreatic neuroendocrine tumors. *Invest Radiol* 2015;50:792–7.
- [28] Yang SH, Lin J, Lu F, et al. Evaluation of antiangiogenic and antiproliferative effects of sorafenib by sequential histology and intravoxel incoherent motion diffusion-weighted imaging in an orthotopic hepatocellular carcinoma xenograft model. *J Magn Reson Imaging* 2017;45:270–80.
- [29] Song YS, Park CM, Lee SM, et al. Reproducibility of histogram and texture parameters derived from intravoxel incoherent motion diffusion-weighted MRI of FN13762 rat breast carcinomas. *Anticancer Res* 2014;34:2135–44.
- [30] Pekar J, Moonen CT, van Zijl PC. On the precision of diffusion/perfusion imaging by gradient sensitization. *Magn Reson Med* 1992;23:122–9.